orientation factors in its orientation image while the anisotropic one only includes one unique angle.

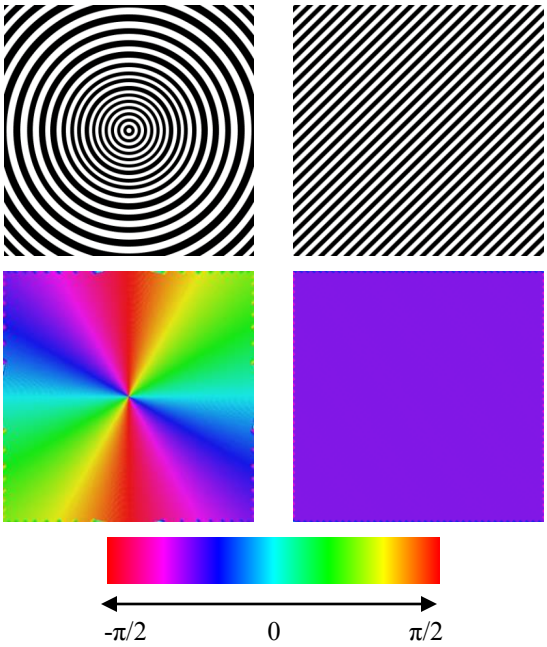

Fig. 3. Example of orientation images calculation. Upper-left to bottom-right: perfectly isotropic texture, anisotropic texture, orientation images of the textures and the palette used to represent the orientation images.

IV. Results

This section presents results of the proposed algorithm using a set of 64 X-ray images. Note that the images are of 400×400 size and with a 16-bit per pixel gray level resolution. ROIs were located on bone areas that contain only a trabecular network.

Figure 4 shows, from top to bottom, the ROI of two X-ray images relative to normal bone (N_1) and fractures bone (F_1), $HRot_0$ of N_1, $HRot_0$ of F_1, $HRot_{90}$ of N_1 and $HRot_{90}$ of F_1. It can be seen that the histogram of the orientation image of N_1 is almost equalized since N_1 is isotropic and includes all the orientation angles. On the contrary, the histogram of F_1 is not equalized and presents main orientation factors highlighted in red. These orientations represent the direction of the compression trabeculae due to the fact that the tensile trabeculae has disappeared, and therefore, F_1 is anisotropic. The histograms of the orientation images of the initial and the rotated version of N_1 are almost similar. On the contrary, those of F_1 are different. As a result, the obtained Kullback–Leibler divergence for N_1 is $KL_{N1}(HRot_0, HRot_{90}) = 0.4124$, and that of F_1 is $KL_{F1}(HRot_0, HRot_{90}) = 0.6223$ which verifies that the proposed algorithm succeeded in detecting that N_1 is relative to normal bone and F_1 is an ROI of fractures bone.

Results on X-ray images of the heel, relative to normal bone, and the pelvis, relative to fractures bone, are shown in Figure 5. The first row of the figure shows the X-ray images while the second row shows the corresponding ROI images N_2 and F_2. The Kullback–Leibler divergence results are the following: $KL_{N2}(HRot_0,HRot_{90})=0.3112$ and $KL_{F2}(HRot_0, HRot_{90})=0.8102$.

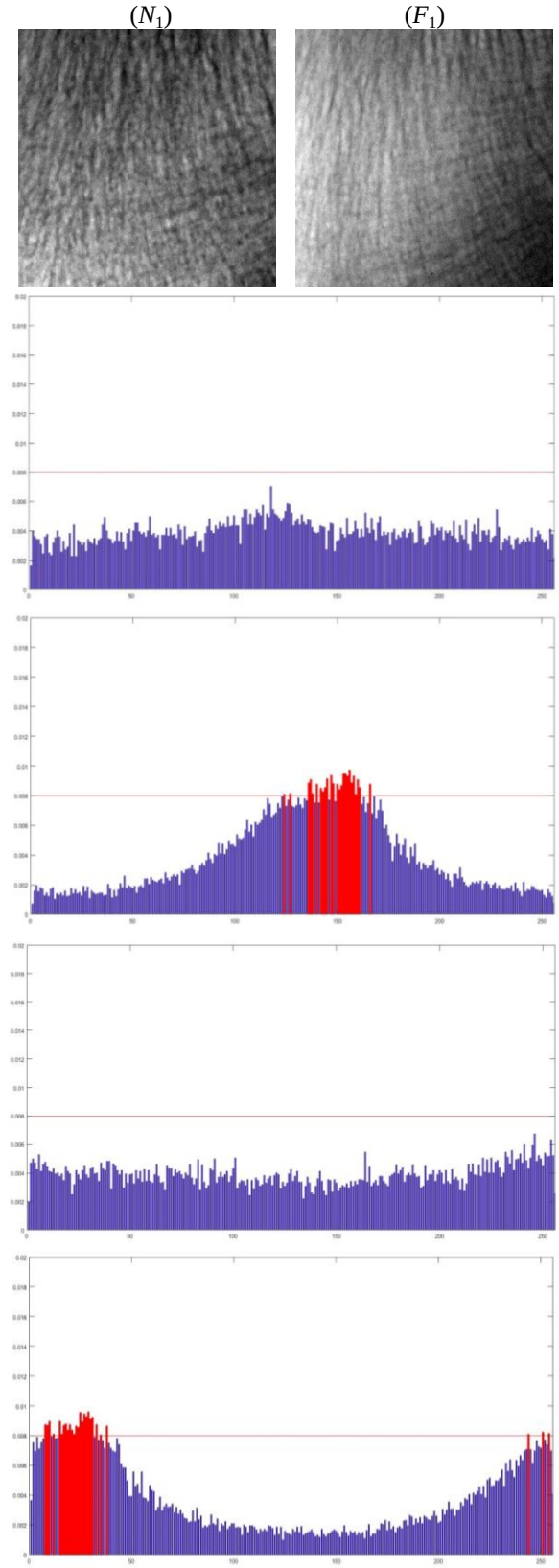

Fig. 4. Practical results. Top to bottom: ROI of X-ray images of normal (N_1) and fractures (F_1) bones. $HRot_0$ of N_1, $HRot_0$ of F_1, $HRot_{90}$ of N_1 and $HRot_{90}$ of F_1.

https://doi.org/10.17758/EARES5.EAP0319210

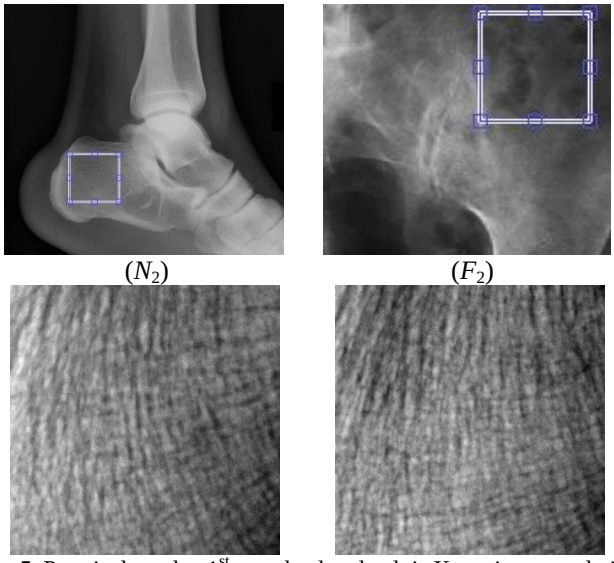

(N_2) (F_2)

Fig. 5. Practical results. 1st row: heel and pelvis X-ray images relative to normal and fractures bone, respectively. 2nd row: ROI textures of the images of the 1st row.

Table 1 summarizes the results obtained by the proposed algorithm on 60 X-ray images. Thirty images relative to normal bone are denoted by N_α and thirty other images relative to fractures bone are denoted by F_α, where α is the number of the image. For all the results, the standard deviation values of the fields of second-moment matrices and the gradient fields are $\sigma_Q = 1$ and $\sigma_H = 1.2$. It can be seen in table 1 that, except for images N_{10}, N_{12}, N_{15}, N_{23}, N_{27}, F_4, F_8, F_{15} and F_{31}, the proposed approach succeeded in accurately differentiating between normal and fractures bone. In other words, the method led to satisfactory estimation of osteoporosis in 85% of the cases.

V. Conclusion

Early work on isotropy estimation does not deal great with local structural variations. Therefore, we proposed a structure-based image isotropy estimation method where the structure layer of the images is represented by the second-moment matrix which gives information about the local orientation and the energy. Applied on different X-ray images, the proposed approach shows that it succeeds in accurately detecting the isotropy/anisotropy of the underlying images, leading to an accurate estimation of bone fractures. As for future perspectives, we aim at adapting the proposed approach to be able to detect other bone diseases by analyzing the texture of the X-ray images.

Acknowledgment

This project has been jointly funded with the support of the National Council for Scientific Research in Lebanon CNRS-L and the Holy Spirit University of Kaslik.

TABLE I: Results of the Proposed Algorithm on 60 X-ray Images

Image	$KL(HRot_0, HRot_{90})$	*Image*	$KL(HRot_0, HRot_{90})$
N_3	0.2112	F_3	0.5992
N_4	0.3251	F_4	0.1511
N_5	0.4512	F_5	0.7465
N_6	0.1112	F_6	0.8576
N_7	0.3145	F_7	0.898
N_8	0.2212	F_8	0.2112
N_9	0.3121	F_9	0.9845
N_{10}	0.7661	F_{10}	0.8756
N_{11}	0.3112	F_{11}	0.7645
N_{12}	0.8475	F_{12}	0.6565
N_{13}	0.3465	F_{13}	0.956
N_{14}	0.4012	F_{14}	0.878
N_{15}	0.712	F_{15}	0.4991
N_{16}	0.1698	F_{16}	0.9421
N_{17}	0.2974	F_{17}	0.9917
N_{18}	0.1999	F_{18}	0.8475
N_{19}	0.347	F_{19}	0.884
N_{20}	0.3415	F_{20}	0.9254
N_{21}	0.2241	F_{21}	0.7656
N_{22}	0.2012	F_{22}	0.925
N_{23}	0.6601	F_{23}	0.9877
N_{24}	0.4001	F_{24}	0.899
N_{25}	0.3521	F_{25}	0.9874
N_{26}	0.227	F_{26}	0.8569
N_{27}	0.5011	F_{27}	0.6325
N_{28}	0.2687	F_{28}	0.5412
N_{29}	0.3404	F_{29}	0.9845
N_{30}	0.1002	F_{30}	0.5991
N_{31}	0.202	F_{31}	0.484
N_{32}	0.3341	F_{32}	0.9861

References

[1] C. Zhu, "Remote sensing image texture analysis and classification with wavelet transform," *Zhengzhou Institute of surveying and mapping*, Zhengzhou 450052, China.

[2] K. Wikantika, A. Harto, and R. Tateishi, "The use of spectral and textural features from Landsat TM image for land cover classification in mountainous area," *Proc. of the IECL Japan workshop*, Tokyo, 2001.

[3] S. Ghanavati, J. Li, T. Liu, P. S Babyn, W. Doda, and G. Lampropoulos, "Automatic brain tumor detection in magnetic resonance images," *ISBI*, 2012.
https://doi.org/10.1109/ISBI.2012.6235613

[4] T. Sugimoto, S. Katsuragawa, T. Hirai, R. Murakami, and Y. Yamashita, "Computerized detection of metastatic brain tumors on contrast-enhanced 3D MR images by using a selective enhancement filter," *World Congress on Medical Physics and Biomedical Engineering*, 2010.

[5] R. Ambrosini and P. Wang, "Computer-aided detection of metastatic brain tumors using automated three-dimensional template matching," *Journal of MRI*, vol. 31, no. 1, pp. 85-93, 2010.
https://doi.org/10.1002/jmri.22009

[6] N. Ray, B. N. Saha, and M. Brown, "Locating brain tumors from MR imagery using symmetry," *Asilomar SSC*, 2007.
https://doi.org/10.1109/ACSSC.2007.4487200

[7] E. M. Lewiecki and J. L. Borges, "Bone density testing in clinical practice," *Arq. Bras Endocrinol Metab.*, vol. 50, no. 4, pp. 586–595, 2006.
https://doi.org/10.1590/S0004-27302006000400004

[8] B. D. Testing, "Bone basics common risk factors for bone loss and osteoporosis," vol. 1, no. 800, pp. 1–5, 2013.

[9] K. Harrar, R. Jennane, K. Zaouchi, T. Janvier, H. Toumi and E. Lespessaille, "Oriented fractal analysis for improved bone

microarchitecture characterization," *Biomedical Signal Processing and Control*, vol. 39, pp. 474-485, 2018.
https://doi.org/10.1016/j.bspc.2017.08.020

[10] C. L. Benhamou, E. Lespessaille, G. Jacquet, R. Harba, R. Jennane, T. Loussot, D. Tourliere, and W. Ohley, "Fractal organization of trabecular bone images on calcaneus radiographs," *Journal of Bone and Mineral Research*, vol. 9, bo. 12, pp. 1909-19018, 1994.

[11] A. S. Saied, A. Saleh, and S. Mohamed, *University of Huddersfield Repository*, 2015.

[12] H. Oulhaj, M. Hassouni, A. Amine, M. Rziza, and R. Jennane, "Fully anisotropic morlet transform for the study of the trabecular bone texture variations," *Proc. ACM Symp. Appl. Comput*, pp. 164-169, 2017.
https://doi.org/10.1145/3019612.3019647

[13] B. Brunet-Imbault, G. Lemineur, C. Chappard, R. Harba, and C.-L. Benhamou, "A new anisotropy index on trabecular bone radiographic images using the fast Fourier transform," *BMC Med. Imaging*, vol. 5, no. June, p. 4, 2005.
https://doi.org/10.1186/1471-2342-5-4

[14] G. Preethi and V. Sornagopal, "MRI Image Classification Using GLCM Texture Features," *Int. Conf. Green Comput. Commun. Electr. Eng. (ICGCCEE)*, pp. 1–6, 2014.
https://doi.org/10.1109/ICGCCEE.2014.6922461

[15] V. Kumar and P. Gupta, "Importance of Statistical Measures in Digital Image Processing," *Int. J. Emerg. Technol. Adv. Eng.*, vol. 2, no. 8, pp. 56–62, 2012.

[16] Fazal-E-Malik and B. Bin Baharudin, "Mean and standard deviation features of color histogramusing laplacian filter for content-based image retrieval," *J. Theor. Appl. Inf. Technol.*, vol. 34, no. 1, pp. 1–7, 2011.

[17] A. Akl, C. Yaacoub, M. Donias, J.-P. Da Costa, and C. germain, "Texture Synthesis using the Structure Tensor.," *IEEE Trans. on Image Processing*, vol. 24, no. 11, pp. 4082-4095, 2015.
https://doi.org/10.1109/TIP.2015.2458701

[18] A. Akl, C. Yaacoub, M. Donias, J.P. Da Costa, and C. Germain, "Structure tensor based synthesis of directional textures for virtual material design," *Proc. of the 21st IEEE International Conference on Image Processing (ICIP)*, October 2014.
https://doi.org/10.1109/ICIP.2014.7025986

[19] A. Akl, C. Yaacoub, M. Donias, J.P. Da Costa, and C. Germain, "Two-stage color texture synthesis using the structure tensor field," *Proc. of the 10th International Joint Conference on Computer Vision, Imaging and Computer Graphics Theory and Applications (VISIGRAPP)*, March 2015.

[20] A. Hassani, M. Hassouni, R. Jennane, M. Rziza, and E. Lespessailles, "Texture analysis for trabecular bone X-ray images using anisotropic Morlet wavelet and Renyi entropy," *Proc. of the 5th International Conference on Image and Signal Processing*, pp. 290-297, 2012.
https://doi.org/10.1007/978-3-642-31254-0_33

[21] K. Harrar, L. Hamami, E. Lespessailles and R. Jennane, "Piecewise whittle estimator for trabecular bone radiograph," *Biomedical signal processing and control*, vol. 8, pp. 657-666, 2013.
https://doi.org/10.1016/j.bspc.2013.06.009

[22] S. Kullback and R. A. Leibler, "On information and sufficiency," *Ann. Math. Statist.*, vol. 22, no. 1, pp. 79–86, Mar. 1951.
https://doi.org/10.1214/aoms/1177729694

A. Akl received the Engineering degree in computer and communications from the Holy Spirit University of Kaslik (USEK), Lebanon, in 2012, and the Ph.D. in signal and image processing from the University of Bordeaux, France, in 2016. His current research interests include image processing, mainly the analysis and synthesis of orientation and tensor-valued spatial processes and their applications to textures and volumes.